Int J Adv Manuf Technol (2012) 60:923–932
DOI 10.1007/s00170-011-3661-3

ORIGINAL ARTICLE

# A dynamic threshold-based fuzzy adaptive control algorithm for hard sphere grinding

**Dongdong Li · Mingming Xu · Chenjun Wei · Dejin Hu · Liming Xu**

Received: 26 June 2011 / Accepted: 20 September 2011 / Published online: 4 October 2011


**Abstract** Grinding wheel wearing fast and metal adhering were severe in hard sphere grinding, which led to wheel overload and clogging. If a fixed-feed grinding was used, the normal pressure between the workpiece and the grinding wheel increased rapidly. Once the grinding load on the grinding wheel was greater than the strength of the retaining bond bridges, a large amount of grains dropped out, which can even damage the wheel. This led to the sphere surface to be scratched. In this study, a dynamic threshold-based fuzzy adaptive control algorithm (DTbFACA) is proposed for hard sphere grinding to avoid scratches on the workpiece. The grinding force was indirectly obtained by measuring the motorized spindle current which was used as a feedback to control hard sphere grinding process. The current threshold in DTbFACA was obtained and online-rectified automatically. The depth of cut and the cup wheel swing speed that affect the motorized spindle current was online-adjusted by fuzzy algorithm. The experimental results indicated that DTbFACA can avoid scratches on the workpiece without sacrificing the sphere form error and grinding efficiency. DTbFACA has been implemented on MD6050 sphere grinding machine tool in production.

**Keywords** Fuzzy adaptive control algorithm · Dynamic threshold · Hard sphere grinding

**Nomenclature**

| | |
|---|---|
| $P_{ch}$ | Chip formation power |
| $P_{pl}$ | Plowing power |
| $P_{sl}$ | Sliding power |
| $d_s$ | Cup wheel diameter |
| $v_s$ | Cup wheel linear velocity |
| $v_w$ | Workpiece rotation speed |
| $v_f$ | Feed rate |
| $a_p$ | Depth of cut |
| DN | Sphere nominal diameter |
| $v_b$ | Cup wheel swing speed |
| $N_{ppw}$ | Number of grinding path per workpiece |
| $I_r$ | Current threshold |
| $a_1$ | Adjusted coefficient of $I_r$ |
| $I_\phi$ | Motorized spindle current range |
| $I_e$ | Motorized spindle rated current |
| $I_{r_0}$ | Initial value of the current threshold |
| $a_{p_0}$ | Initial value of $a_p$ |
| $v_{b_0}$ | Initial value of $v_b$ |
| $a_2$ | Adjusted coefficient of $a_p$ |
| $a_3$ | Adjusted coefficient of $v_b$ |
| $E_i$ | Linguistic variable of $e$ (error) |
| $E_j$ | Linguistic variable of ec (change of the error) |
| $U_{n(i,j)}$ | linguistic variable of $u$ (output control signal) |
| $k_u$ ($u$=1, 2, 3) | Output scaling factor |
| $D$ | Sphere diameter |
| $(x_0, y_0, z_0)$ | Center coordinate parameters of the sphere |
| $(x_i, y_i, z_i)$ | Coordinates of the $i$th sampling point |
| $R_1$ | Sphere radius before grinding |
| $R_2$ | Sphere radius after grinding |
| $t_1$ | Grinding time |
| $F_N$ | Applied normal force |
| $F_{TH}$ | Lower limit of the normal force below which no significant amount of material removal takes place |
| $K_p$ | Coefficient of the grinding wheel and workpiece |

D. Li (✉) · M. Xu · C. Wei · D. Hu · L. Xu
School of Mechanical Engineering,
Shanghai Jiao Tong University,
Shanghai 200030, China
e-mail: ddl06@yahoo.com.cn

## 1 Introduction

Metallic hard sealing spherical valve, which can resist high temperature up to 500°C, high pressure up to 30 MPa, corrosion, and wear, is most widely used in petroleum chemical engineering, metallurgy, coal liquefaction engineering and nuclear power engineering [1]. As a key part of the spherical valve, the sphere must have high hardness (HRC≥60) and precision to work in harsh environment. The sphericity error of the sphere must be less than 0.02 mm, and the sphere surface roughness must be less than 0.2 μm. To obtain high surface hardness, WC-Co, Ni60, and other hard alloys are sprayed onto the sphere substrate to reach a coating depth of 0.4–0.6 mm. The sphere must be ground after coating to meet the requirements of the form accuracy. The sphere surface roughness ($R_a$) must be less than 0.4 μm after grinding. It can reach less than 0.2 μm after the sphere lapping in with the valve seat in the last sphere manufacturing step. As the coating materials WC-Co, Ni60, and other hard alloys have high hardness, low modulus of elasticity, great ductility, and impact resistance, the grinding wheel wore fast and the metal adhesion was severe in hard sphere grinding, which can lead to wheel overload and clogging. If a fixed-feed grinding (FFG) was used, the normal pressure between the workpiece and the grinding wheel increased rapidly. Once the grinding load on the grinding wheel was greater than the strength of the retaining bond bridges, a large amount of grains dropped out, which can even crush the grinding wheel. This led to the sphere surface to be scratched. The depth of the scratches can reach 0.2 mm which can result in the scrapping of the workpiece. Consequently, methods must be taken to control the grinding process.

Grinding force, grinding power, acoustic emission signal, acceleration, and temperature are always used as feedback for grinding process monitoring and control. It has not changed much in recent years. However, the advent of artificial intelligence (AI) for the design of the controller has had a significant effect on the grinding process, which can improve the grinding efficiency and the workpiece quality [2–5]. In the field of grinding, a variety of approaches have been employed such as knowledge-based system, expert system, fuzzy logic, neural networks, genetic algorithm, and adaptive control optimization (ACO). From the viewpoint of AI, ACO is an integration of a knowledge-based system into a controller. It has the capabilities such as sensing and monitoring process parameters and uses rules and models to optimize the process and adaptively control the process [2].

ACO systems with such features have been developed by many researchers. Amitay et al. [3] investigated a computerized adaptive control grinding system to optimize both grinding and dressing conditions. Its performance is demonstrated by the experiment on 1,045 steels. The system is based upon online convergence along a predetermined optimal trajectory derived from grinding theory. As the hard sphere grinding theory is not clear as cylindrical grinding, it is difficult to use this system in hard sphere grinding. König et al. [6] investigated a direct adaptive control strategy in plunge grinding process using AE sensor. However, the application of the strategy needs the experimentally calibrated empirical models.

Kelly et al. [4] proposed a control system framework suitable for adaptive control of the grinding process. An adaptive fuzzy neural network control system in cylindrical grinding process was proposed by Li and Ding [5]. However, both of the control strategies suggested by the researchers use the economic database or the expert knowledge. To obtain a satisfied economic database or the expert knowledge is difficult in practice.

Wang [7] described an ACC fuzzy logic controller for cylindrical traverse grinding which optimizes the grinding power. Lu and Dong [8] used the artificial intelligence control strategy to control the grinding force in the ceramic grinding process. The grinding processes have been improved by the strategies. However, a fixed power (force) threshold must be set before grinding. It is difficult to set a proper threshold to satisfy different grinding conditions.

It can be concluded that none of these studies has investigated the application of the adaptive control systems into sphere grinding and that the adaptive control system stated above cannot be directly used in sphere grinding on various grinding conditions. The application and operability of these adaptive control systems are restricted. To date, the adaptive control systems stated above are seldom utilized in industrial or practical applications. Besides, these adaptive control systems are too complex and vary greatly from one to another. In practice, simple and easy-to-handle control systems might often be preferable. In this paper, a dynamic threshold-based fuzzy adaptive control algorithm (DTbFACA) is introduced to stabilize the grinding process in hard sphere grinding.

## 2 Grinding power-related parameters of hard sphere grinding

### 2.1 Novel sphere grinding machine tool

Figure 1 shows the schematic of novel sphere grinding machine tool. Sphere 17 is fixed by fixture 14. The left end of fixture 14 is clamped by chuck 2 on headstock 1, and the right end of fixture 14 is held by center 15 on tailstock 16. Fixture 14 rotates with sphere 17 by the drive of headstock 1. One end of rotating Table 3 is supported by an arc guide 11. It rotates around pivot 13, which is actuated by a stepper motor 20 through worm 18 and worm wheel 12.

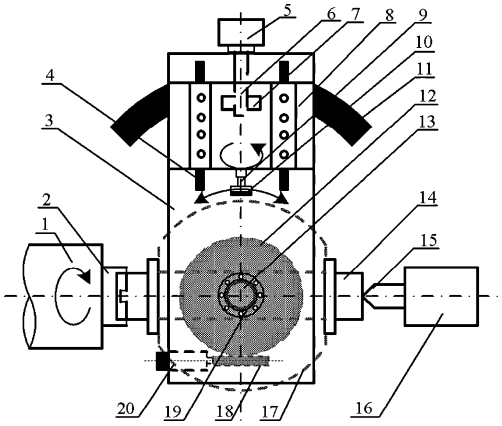


**Fig. 1** Novel sphere grinding machine tool. *1* headstock, *2* chuck, *3* rotating table, *4* linear guide, *5* stepper motor, *6* ball screw, *7* nut, *8* moving table, *9* motorized spindle, *10* cup wheel, *11* arc guide, *12* worm wheel, *13* pivot, *14* fixture, *15* center, *16* tailstock, *17* sphere, *18* worm, *19* bearing, *20* stepper motor

Motorized spindle 9 is mounted on moving table 8. The movement of moving table 8 is provided by a ball screw 6 which is actuated by a stepper motor 5 through coupling. A nut 7 connects ball screw 6 and moving table 8. Cup wheel 10 is mounted on the shaft of motorized spindle 9. In the sphere grinding process, sphere 17 rotates along with fixture 14. The rotation of cup wheel 10 is provided by motorized spindle 9. Cup wheel 10 also rotates around pivot 13, and the feed motion of cup wheel 10 is provided by stepper motor 5. The cup wheel that the diameter is smaller than the sphere diameter can be used in this machine tool, and NC interpolation is not needed.

## 2.2 Grinding power

The measurement of grinding power is technically easier compared with grinding force, acoustic emission, acceleration, and temperature, and grinding power is proportional to grinding force [7, 9]. Depending on the type of system used, current, voltage, and phase shift can be respectively detected. The installation of the sensors does not change the machine tool structure and has no negative impact on the process. The amount of investment is also very moderate, which makes this sensor type attractive for industrial application. It is even possible to gain information about the actual power from the drive system of machine tools without additional sensors [10].

There is a direct relationship between the grinding power and the magnitude of the dull wear flat area. For most practical grinding operations, the grinding power progressively increases due to wheel dulling. This is a time-dependent behavior. Grinding power consists of chip formation, plowing, and sliding components [11, 12]:

$$P = P_{\mathrm{ch}} + P_{\mathrm{pl}} + P_{\mathrm{sl}}\{A_{\mathrm{eff}}\} \tag{1}$$

The time-dependent behavior due to dulling is manifested in the sliding power, which is proportional to the effective wear flat area $A_{\mathrm{eff}}$. During grinding, $A_{\mathrm{eff}}$ grows from its initial value $A_{\mathrm{eff},0}$ after dressing by $A_{\mathrm{sl}}$ due to the grains sliding against the workpiece [11, 12]:

$$A_{\mathrm{eff}} = A_{\mathrm{eff},0} + A_{\mathrm{sl}} \tag{2}$$

$A_{\mathrm{eff}}$ increases fast and metal adhesion is so strong in hard sphere grinding, which leads to the grinding power increase rapidly. So the grinding power is utilized to monitor the hard sphere grinding process.

The motorized spindle used in novel sphere grinding tool is an alternating current asynchronous motor. It is driven by the inverter of YASKAWA (F7B4018). The control mode of the inverter is *V/f*. The output voltage is a constant when the frequency does not change under the *V/f* mode. The output current of the inverter is equal to the motorized spindle current. So the grinding power can be indirectly obtained by measuring the motorized spindle current.

The cup wheel diameter, workpiece material, depth of cut, workpiece rotation speed, cup wheel linear velocity, cup wheel swing speed, and sphere diameter all affected the motorized spindle current in hard sphere grinding. Figure 2 shows the

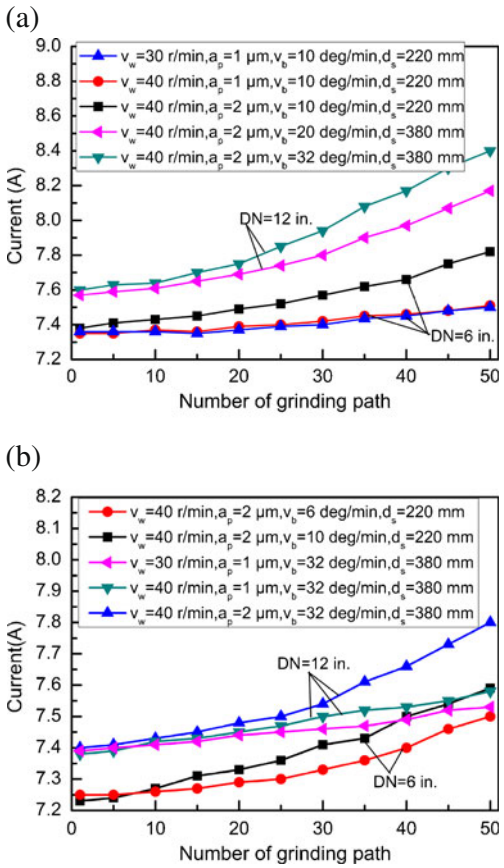


**Fig. 2** Motorized spindle current versus number of grinding path. **a** Workpiece material: WC. **b** Workpiece material: Ni60

motorized spindle current in the sphere grinding using FFG. The coating material of the hard sphere is WC and Ni60 which are most commonly used in valve industry. The ceramic-bonded diamond cup wheel was used, and it was dressed by a resin bonded alumina cup wheel after each sphere was ground. The dressing depth is 10 μm. Table 1 shows the grinding parameters.

Figure 2 shows that the motorized spindle current was not the same at the beginning of the grinding for different sphere diameters. The reason is that the motorized spindle speed must change with the cup wheel diameter to keep the cup wheel linear velocity at the recommended linear velocity 35 m/s. The motorized spindle current increased along with the increase of number of grinding path. The reason seems to be:

1. The cup wheel wore progressively in the grinding process.
2. The material removal rate was low, which led to the grinding power to increase along with the increase of number of grinding path.
3. The thermal expansion of the sphere and the motorized spindle caused the grinding pressure increasing when the sphere and the motorized spindle were not in thermal equilibrium.

Figure 2 also shows that the influence of depth of cut upon motorized spindle current was more significant than the cup wheel swing speed, and the influence of cup wheel swing speed upon motorized spindle current was larger than workpiece rotation speed.

## 3 Dynamic threshold-based fuzzy adaptive control algorithm

From the discussions in Section 2, a conclusion can be drawn that if the motorized spindle current was used as a feedback to control the hard sphere grinding process, it was very difficult to set one fixed current threshold to satisfy the variation of workpiece material, cup wheel diameter, and sphere diameter to stabilize the grinding process. So a dynamic threshold-based fuzzy adaptive control algorithm is developed according to the features of the motorized spindle current discussed in Section 2. The current threshold can be obtained and online-rectified automatically. The workpiece rotation speed had less effect on the motorized spindle current than the depth of cut and the cup wheel swing speed. So the depth of cut and the cup wheel swing speed were chosen to be online-adjusted by the fuzzy algorithm.

**Table 1** Grinding parameters

| Parameter | Value |
|---|---|
| $d_s$ (mm) | 220, 380 |
| $v_s$ (m/s) | 35 |
| $v_w$ (r/min) | 30, 40 |
| $v_f$ (mm/min) | 5 |
| $a_p$(μm) | 1, 2 |
| DN (in.) | 6, 12 |
| $v_b$ (deg/min) | 6, 10, 20, 32 |
| Workpiece material | WC, Ni60 |
| $N_{ppw}$ | 50 |

Figure 3 shows the block diagram of DTbFACA. The grinding force was indirectly obtained by measuring the motorized spindle current, and the motorized spindle current was used as a feedback to control the grinding process.

Figure 4 illustrates the flow chart of DTbFACA, and the working steps are:

1. The initial value of the current threshold $I_{r_0}$ is determined by multiplying the rms current obtained in the second grinding path by a factor $\beta$. $\beta$ was obtained from the experiments in Section 2. It can be described as

$$\beta = I_{o_{max}} / I_{o_{min}} \tag{3}$$

   $\beta$ is equal to 1.09 and 1.05 when the workpiece material is WC and Ni60, respectively, in the experiment in Section 2. Once the maximum $\beta$ is chosen, the grinding process may not be stable when the workpiece material is Ni60. So the minimum value 1.05 is used as the value of $\beta$ in the study.
2. The tool withdraws when the motorized spindle current $I_o$ is greater than the current threshold $I_r$, which can decrease the wheel load. The tool withdrawal distance is $a_p$, and this action is implemented by control the stepper motor 5 in Fig. 1.
3. Calculate the number of the tool advance $N_f$ and the number of the tool withdrawal $N_b$. If $N_b$ is greater than $N_f$, then adjust the current threshold $I_r$; otherwise, the current threshold keeps unchanged.
4. To adjust $a_p$ and $v_b$ in turn as the adjustment number of the current threshold $N_I$ reaches $m$.

At the beginning of the grinding process, the grinding power is small for the wheel load is small and the wheel is

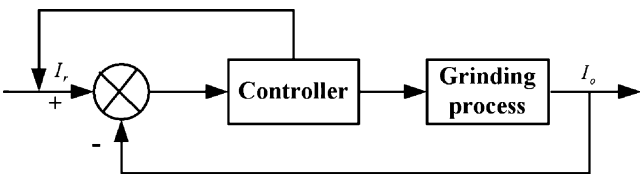


**Fig. 3** Block diagram of DTbFACA

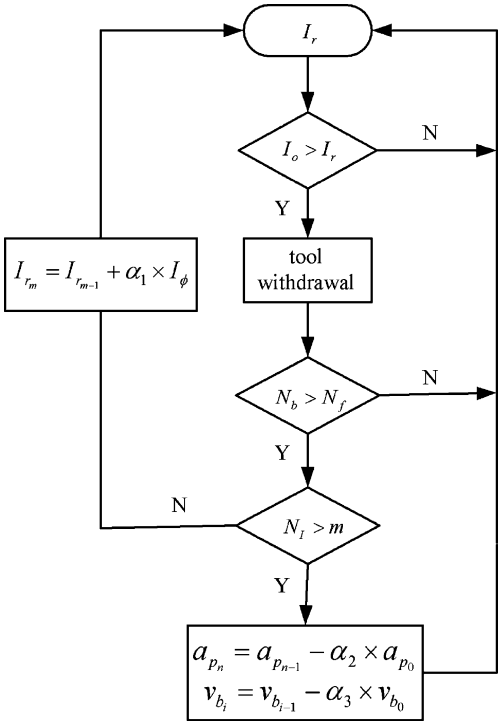


**Fig. 4** Flow chart of DTbFACA

just dressing, and the initial value of the current threshold is gotten at this time. So the current threshold is adjusted firstly. In order not to decrease the grinding efficiency and keep the grinding process stable, a proper current threshold must be found. The adjustment of the current threshold $I_r$ is determined by $N_e$ which can be described as

$$N_e = N_b/N_f \tag{4}$$

The higher the $N_e$, the more the tool withdrawal, which shows the wheel load is higher. The current threshold can be described as

$$I_{r_m} = I_{r_{m-1}} + \alpha_1 \times I_\phi \qquad (m = 1, 2, \cdots N) \tag{5}$$

$I_\phi$ can be described as

$$I_\phi = I_e - I_{r0}$$

The grinding pressure at the time $t$ is equal to $t-1$ approximately when $N_e$ is not greater than 1. During this period, the current threshold is proper and grinding process is stable. The grinding pressure at the time $t$ is larger than the time $t-1$ when $N_e$ is greater than 1. At this time, the current threshold is small, which leads to the increase of the number of tool withdrawal before the adjustment number of current threshold $N_I$ reaches $m$. The grinding pressure reaches a proper value when the adjustment number of current threshold $N_I$ reaches $m$. $m$ cannot be too big; otherwise, the grinding pressure will be too high and the grinding process is not stable.

The adjustment number of current threshold $N_I$ reaches $m$ and $N_e$ is still greater than 1, which indicates the grinding parameter is not proper. In this case, $a_p$ and $v_b$ should be adjusted in turn. The adjustment of $a_p$ can be described as

$$a_{p_n} = a_{p_{n-1}} - \alpha_2 \times a_{p_0} \qquad (n = 1, 2, \cdots N) \tag{6}$$

$a_p$ should not be too small, and it is not smaller than 0.5 μm in practice. The adjustment of $v_b$ is also determined by $N_e$. $v_b$ can be described as

$$v_{b_i} = v_{b_{i-1}} - \alpha_3 \times v_{b_0} \qquad (i = 1, 2, \cdots N) \tag{7}$$

It is very difficult to build an accurate mathematical model for hard sphere grinding process. The fuzzy control algorithm can utilize linguistic rules generated from the human knowledge and experimental data to provide necessary control actions [13]. Therefore, the fuzzy control algorithm is used to adjust $I_r$, $a_p$, and $v_b$, respectively. The fuzzy controller is a basic two-input single-output controller used most in practice shown in Fig. 5.

The two inputs are the error $e$ and the change of the error ec, which are scaled by multiplying suitable scaling factors. Singleton fuzzification and triangular membership shown in Fig. 6 used in [13] are also adopted in this fuzzy controller. The input membership function is the same as the output membership function.

Fuzzy control rules are composed of a series of fuzzy IF–THEN rules. In this study, the fuzzy control rules are in the form of

$$\mathrm{R}: \text{if } e \text{ is } E_i \text{ and ec is } E_j, \text{ then } u \text{ is } U_{n(i,j)}, \tag{8}$$

Table 2 shows a fuzzy rule base defined for each control input. Mamdani's minimum fuzzy implication and center average defuzzification used by Xu and Shin [13] are also adopted in this study. The output control signal $u$ $(\alpha_1, \alpha_2, \alpha_3)$ can be described as

$$u = k_u \times \sum_{i,j} \left\{ [\mu_{E_i}(e) \cap \mu_{E_j}(\mathrm{ec})] U_{n(i,j)} \right\} / \sum_{i,j} [\mu_{E_i}(e) \cap \mu_{E_j}(\mathrm{ec})] \tag{9}$$

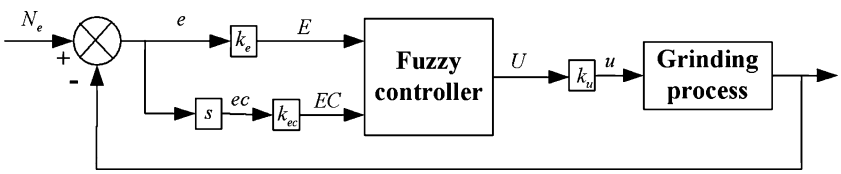


**Fig. 5** Fuzzy controller model

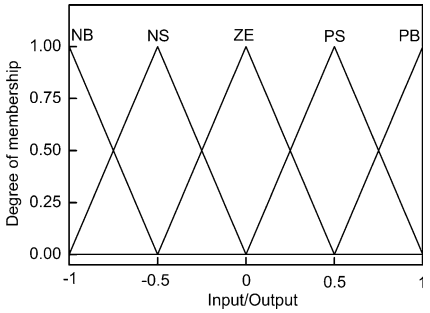


**Fig. 6** Membership function for the fuzzy controller

$\mu_{E_i}(e) \cap \mu_{E_j}(\mathrm{ec})$ indicates the intersection of fuzzy sets $\mu_{E_i}(e)$ and $\mu_{E_j}(\mathrm{ec})$, which is defined as the "min" operation between two fuzzy sets

$$\mu_{E_i}(e) \cap \mu_{E_j}(\mathrm{ec}) = \min\left[\mu_{E_i}(e), \mu_{E_j}(\mathrm{ec})\right] \tag{10}$$

As shown in Fig. 6, the universes of discourse for all inputs and outputs are normalized over the interval [−1, 1]. The scaling factors of the inputs and outputs have an important influence on the performance of the resultant control system [13, 14]. It is not entirely subjective to choose the scaling factors since their magnitude is a compromise between the sensitivity during the required steady state accuracy and the rise time. The principles on how to determine the scaling factors ($k_e$, $k_{\mathrm{ec}}$, and $k_u$) without any mathematical process model have been established by the researchers [13, 15–17]. Suppose the maximum possible error in the grinding process is $e$ and the error can change at most by ec. Then the error scaling factor $k_e$ and the change-in-error scaling factor $k_{\mathrm{ec}}$ can be quantitated as 6.0/$e$ and 6.0/ec. The output scaling factor $k_u$ is chosen to accommodate the controller output to the process input according to [16, 17].

$$k_u = \frac{\text{max process input}}{\text{max controller output}} \tag{11}$$

In this study, the scaling factors were:

$$k_e = 1.33, k_{\mathrm{ec}} = 0.67, k_u(u = 1,\ 2,\ 3) = 0.01,\ 0.075,\ 0.05.$$

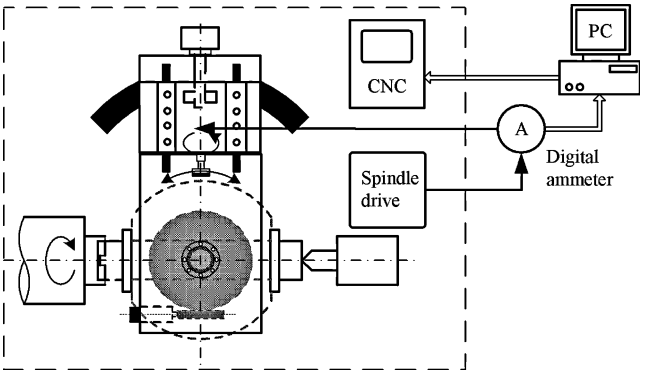


**Fig. 7** Experiment schematic diagram

## 4 Experiments

Experiments were conducted on a MD6050 NC precision sphere grinding machine tool whose schematic is illustrated in Fig. 1. The nominal diameter of the sphere from 1 to 12 in. can be ground using MD6050 NC precision sphere grinding machine tool. Figure 7 shows the experiment schematic diagram.

One-phase current of the motorized spindle was measured by a digital ammeter (DP4-RMSAA20S2). The digital ammeter can measure the current from 1 to 30 A. PC communicates with the digital ammeter by RS232. FFG and DTbFACA were conducted in the experiment. The cup wheel used in the experiment and the dressing condition are the same as in Section 2. Table 3 shows the experiment parameters.

A three-dimensional coordinate measuring machine (CMM) was used to measure the sphericity error. The model of the CMM is IOTA0101DH/T-P and its resolution is 0.5 μm which is produced by Institute of Aviation Precision Mechanics of China. The sampling points are on the intersection of the latitude and longitude. In the measuring process of the sphericity using CMM, the distribution of the sampling can be stochastic. So the distance between the adjacent latitude is nearly the same, and the distance between the adjacent longitudes is also nearly the same. The total sampling points is 50 which is

**Table 2** Fuzzy rules

| $e$ / $a_1/a_2/a_3$ / ec | NB | NS | ZE | PS | PB |
|---|---|---|---|---|---|
| NB | NB/NB/NB | NB/NS/NS | NS/ZE/ZE | ZE/PS/PS | PS/PB/PB |
| NS | NB/NB/NB | NB/NS/NS | NS/ZE/ZE | ZE/PS/PS | PS/PB/PB |
| ZE | NB/NB/NB | NS/NS/NS | ZE/ZE/ZE | PS/PS/PS | PB/PB/PB |
| PS | NB/NS/NS | NS/ZE/ZE | ZE/PS/PS | PS/PB/PB | PB/PB/PB |
| PB | NB/NS/NS | NS/ZE/ZE | ZE/PS/PS | PS/PB/PB | PB/PB/PB |

**Table 3** Experiment parameters

| Parameter | FFG | DTbFACA |
|---|---|---|
| $d_s$ (mm) | 220, 380 | 220, 380 |
| $v_s$ (m/s) | 35 | 35 |
| $v_w$ (r/min) | 40 | 40 |
| $v_f$ (mm/min) | 5 | 5 |
| $a_p$ (μm) | 2 | 2 |
| DN (in.) | 6, 12 | 6, 12 |
| $v_b$ (deg/min) | 10, 32 | 10, 32 |
| $m$ | – | 3 |
| Workpiece material | WC, Ni60 | WC, Ni60 |
| $N_{ppw}$ | 100 | 100 |

suggested in [18]. The CMM can be programmed to operate automatically and a set of point data can be captured. To edit a program to measure the point data is complex. But once the program was successfully proved, it could be quickly revised for the measurement of the different diameter sphere.

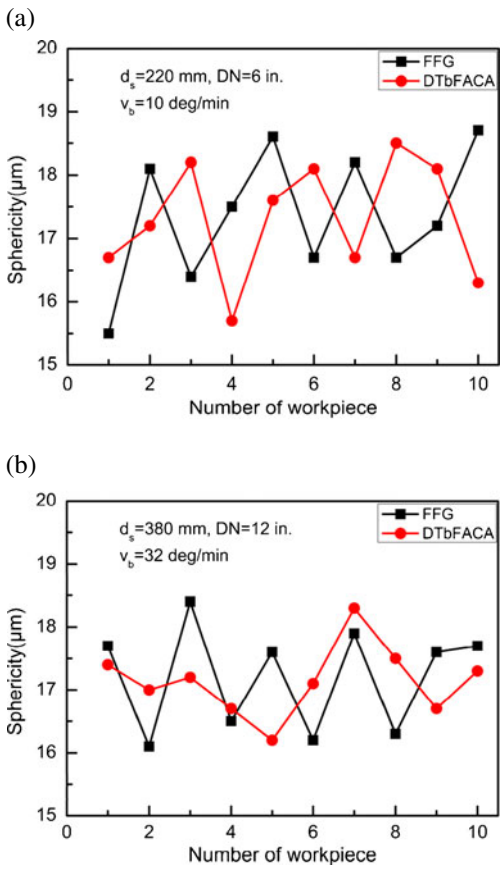


**Fig. 8** Sphericity of the sphere. **a** Workpiece material: WC. **b** Workpiece material: Ni60

The least square methodology is the most frequently applied and most widely accepted fitting algorithm [19–21]. The least square fitting algorithm used in [19–23] is also used in this study to calculate the sphericity error. The sphere equation can be given as

$$(x - x_0)^2 + (y - y_0)^2 + (z - z_0)^2 = (D/2)^2 \tag{12}$$

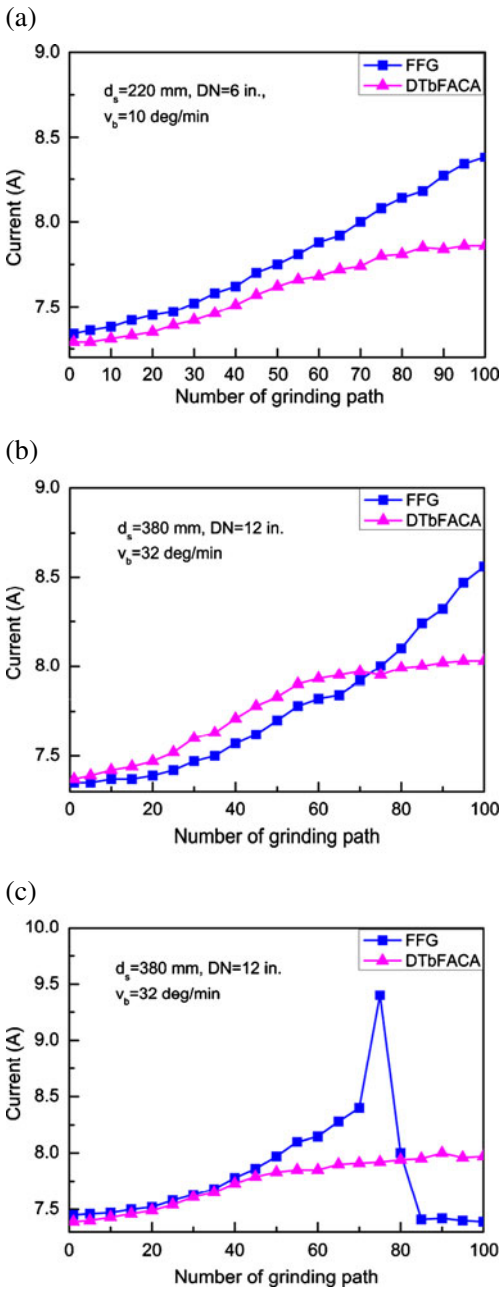


**Fig. 9** Motorized spindle current in the experiment. **a** Workpiece material: WC. **b** Workpiece material: Ni60. **c** Workpiece material: Ni60 (scratches appear)

The objective is to obtain good estimators for $x_0$, $y_0$, $z_0$, and $D$ on the information of the sampling points. The error function for the least square sphere fitting is [20, 21, 24]

$$\delta_i = \min \sum_{i=1}^{n} [\sqrt{(x_i - x_0)^2 + (y_i - y_0)^2 + (z_i - z_0)^2} - (D/2)]^2 \tag{13}$$

The sphericity error is

$$\mathrm{LSS} = \delta_{\max} - \delta_{\min} \tag{14}$$

The sphere radius before and after grinding can be measured by CMM (IOTA0101DH/T-P). So the volume of the sphere can be calculated before and after grinding, and the material removal rate was calculated from the change of the volume of the sphere and the grinding time. The material removal rate can be described as

$$Q = 4\pi(R_1^3 - R_2^3)/3t_1 \tag{15}$$

## 5 Results and discussion

Figure 8 shows the sphericity of the sphere grinding using FFG and DTbFACA. It can be seen that the sphericity is almost unchanged whether the sphere grinding using FFG and DTbFACA. The reason seems to be

1. The number of tool withdrawal is few.
2. The material removal rate is low, which will lead to the number of tool withdrawal has little effect on the sphere form error.

Figure 9 shows the motorized spindle current in the sphere grinding using FFG and DTbFACA. It can be seen from Fig. 9a, b the motorized spindle current increases along with the number of grinding path in the sphere grinding using FFG. The motorized spindle current increases slowly when it is greater than the current threshold in the sphere grinding using DTbFACA. If the grinding pressure is not controlled in the sphere grinding using FFG, the motorized spindle current will increase continuously. In this case, a large amount of grain will be dropped out from the cup wheel and the sphere surface will be scratched, even as far as the grinding wheel to be crushed. As the grinding parameter is the same, the motorized spindle current shown in Fig. 9 is not the same at the beginning of the grinding. The reason is that the coating hardness is not the same with the same coating spray metal and operation, and the tool setting is different in every grinding process.

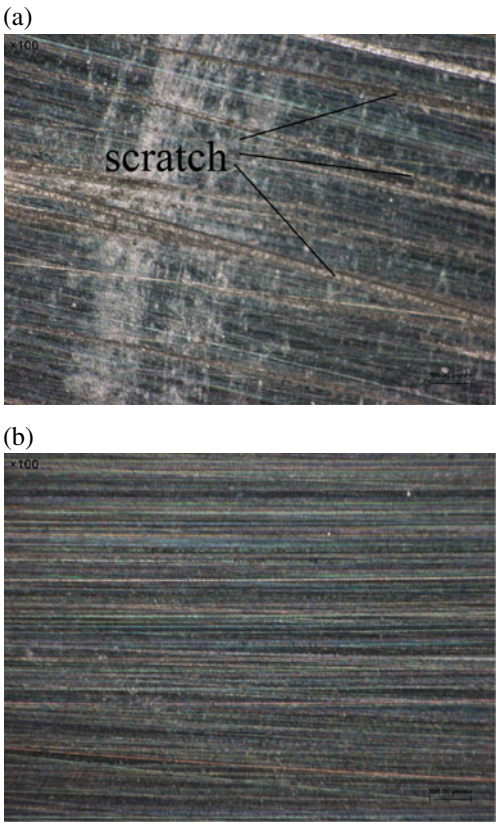


**Fig. 10** **a** Sphere surface with scratches and **b** normal sphere surface

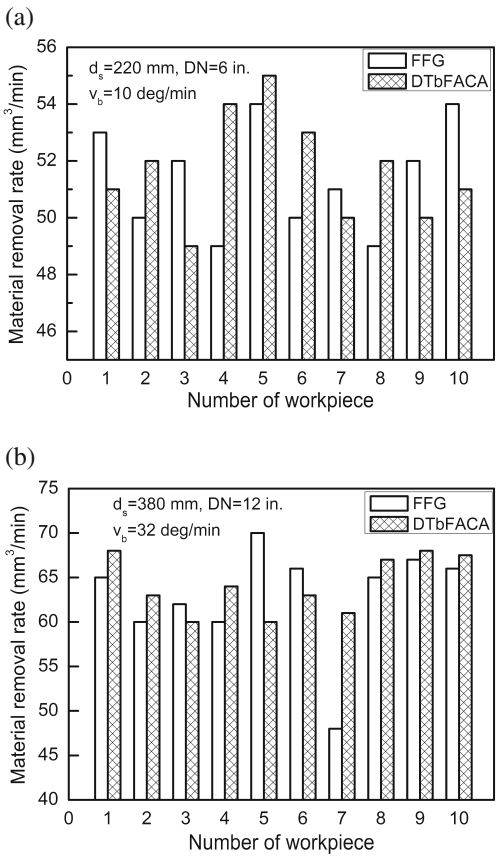


**Fig. 11** Material removal rate. **a** Workpiece material: WC. **b** Workpiece material: Ni60

Figure 9c shows the motorized spindle current increases firstly and reduces afterward in the sphere grinding using FFG, which is different from Fig. 9a, b. In this grinding process, a large noise occurred as the grinding wheel was crushed. The motorized spindle current increased before the cup wheel was crushed, and it decreased as the cup wheel did not touch with the sphere after the cup wheel was crushed. Figure 10 shows the sphere surface with scratches and the normal sphere surface. It can be seen that a lot of scratches was on the sphere surface in Fig. 10a. This made the surface roughness poor.

Figure 11 shows the material removal rate measured in the experiment. It can be seen that the material removal rate does not decrease in the sphere grinding using DTbFACA by comparing with the sphere grinding using FFG. The material removal rate can be described as [25]:

$$Q = K_p(F_N - F_{TH})v_s \tag{16}$$

$K_p$ and $F_{TH}$ represent the current condition of the specific grinding wheel and workpiece. From Eq. 16, it can be seen the material removal rate $Q$ increases along with $F_N$ as $K_p$ and $v_s$ do not change. In the sphere grinding using FFG, $F_N$ increases along with the number of grinding path. The more $F_N$ increase, the more the grinding wheel wear. In this case, $K_p$ decreases and $Q$ is not always increase. In the sphere grinding using DTbFACA, $F_N$ is not always increasing along with the number of grinding. The grinding wheel wear may less than the sphere grinding using FFG. So the material removal rate $Q$ is almost the same as the sphere grinding using FFG. It can be seen from Fig. 11b that the material removal rate in the sphere grinding using DTbFACA is greater than the sphere grinding using FFG when grinding the seventh workpiece. The reason was that the cup wheel was crushed in the sphere grinding using FFG.

## 6 Conclusions

The sphere grinding using DTbFACA can avoid the scratches on the workpiece without sacrificing the sphere form error and the grinding efficiency by comparing with the sphere grinding using FFG. It did not need any database or expert knowledge compared to the researches [4, 5]. The current threshold in DTbFACA can be obtained and online-rectified automatically, which was easier to be used in practice compared to researches [7, 8]. DTbFACA for hard sphere grinding had better operability and versatility compared to other control algorithms, and it can be used in commercial systems. It is also easy to be modified to suit other grinding process.

**Acknowledgments** This research is sponsored by the National Natural Science Foundation (no. 51075273), State Key Lab of Digital Manufacturing Equipment & Technology of Huazhong University of Science and Technology (no. 2008-DMET-KF-001), and State Key Laboratory of Mechanical System and Vibration of Shanghai Jiao Tong University (no. MSVMS201104).

## References

1. Wu Q (2006) Research on precision grinding technology in machining high rigidity rotary sphere. Dissertation, Shanghai Jiao Tong University, Shanghai, China
2. Rowe WB, Li Y, Mills B, Allanson DR (1996) Application of intelligent CNC in grinding. Computers in industry 31:45–60
3. Amitay G, Malkin S, Karen Y (1981) Adaptive control optimization of grinding. Journal of Engineering for Industry 103 (1):103–108
4. Kelly S, Rowe WB, Moruzzi JL (1989) Adaptive grinding control. Advanced Manufacturing Engineering 1(5):287–295
5. Li XM, Ding N (2010) Adaptive fuzzy neural network control system in cylindrical process. Key Engineering Materials 426–427:220–224
6. König W, Altintas Y, Memis F (1995) Direct adaptive control of plunge grinding process using acoustic emission sensor. International Journal of Machine tools & Manufacture 35 (10):1445–1457
7. Wang JZ (2006) Study on the key techniques of intelligent cylindrical traverse grinding. Dissertation, Jilin University, Jilin, China
8. Lu YY, Dong JH (2010) The study of force control with artificial intelligence in ceramic grinding process. Intelligence Information Processing and Trusted Computing (IPTC), 2010 International Symposium on 208–211
9. Chen X, Rowe WB, Allanson DR, Mills B (1999) A grinding power model for selection of dressing and grinding condition. Journal of Manufacturing Science and Engineering 121:632–637
10. Tönshoff HK, Friemuth T, Becker JC (2002) Process monitoring in grinding. Manufacturing Technology 51(2):551–571
11. Malkin S, Guo CS (2008) Grinding technology: theory and application of machining with abrasives, 2nd edn. Industrial, New York
12. Xiao G, Malkin S (1996) On-line optimization for internal plunge grinding. Manufacturing Technology 45(1):287–292
13. Xu CY, Shin YC (2007) Control of cutting force for creep-feed grinding processes using a multi-level fuzzy controller. Journal of Dynamic Systems Measurement and Control 129(4):480–493
14. Lee CC (1990) Fuzzy logic in control systems: fuzzy logic controller-part I. System, Man and Cybernetics 20(2):404–418
15. Hsu PL, Fann WR (1996) Fuzzy adaptive control of machining processes with a self-learning algorithm. Journal of Manufacturing Science and Engineering 118(4):522–530
16. Linkens DA, Abbod MF (1992) Self-organising fuzzy logic control and the selection of its scaling factors. Transactions of the Institute of Measurement and Control 14(3):114–125
17. Linkens DA, Abbod MF (1991) Self-organising fuzzy logic control for real time processes. International Conference on Control 2:971–976
18. He GY, Wang TY, Zhao J, Yu BQ, Li GQ (2006) Algorithm for sphericity error and the number of measured points. Chinese Journal of Mechanical Engineering 19(3):460–463
19. Cui CC, Fu SW, Huang FG (2009) Research on the uncertainties from different form error evaluation methods by CMM sampling. International Journal of Advanced Manufacturing Technology 43:136–145

20. Jung M, Cross KJ, McBride JW, Hill M (2000) A method for the selection of algorithm for form characterization of nominally spherical surfaces. Precision Engineering 24:127–138
21. Chen KW, Papadoupoulos AS (1996) Comparison of the linear least squares and nonlinear least squares spheres. Microelectronics and Reliability 36(1):37–46
22. Liu B, Xu LM, Chai YD, Xu KZ, Dd L (2011) On-site measurement of sphericity based on high-precision sphere grinder. Journal of Shanghai Jiaotong University 45(1):66–70
23. Samuel GL, Shunmugam MS (2003) Evaluation of circularity and sphericity from coordinate measurement data. Journal of Materials Processing Technology 139:90–95
24. Zhu XS, Ren XS, Yang JG, Xue BY (1998) General formula for the least square sphericity. Journal of Shanghai Jiaotong University 32(5):43–45
25. Jenkins HE, Kurfess TR (1999) Adaptive pole-zero cancellation in grinding force control. Control Systems Technology 7 (3):363–370